Depth estimation for speckle projection system using progressive reliable points growing matching

Guijin Wang,* Xuanwu Yin, Xiaokang Pei, and Chenbo Shi

Department of Electronic Engineering, Tsinghua University, Beijing 100084, China

*Corresponding author: wangguijin@tsinghua.edu.cn

Received 31 July 2012; revised 23 October 2012; accepted 14 November 2012;
posted 11 December 2012 (Doc. ID 173553); published 18 January 2013

In this paper, we propose a progressive reliable points growing matching scheme to estimate the depth from the speckle projection image. First a self-adapting binarization is introduced to reduce the influence of inconsistent intensity. Then we apply local window-based correlation matching to get the initial disparity map. After the initialization, we formulate a progressive updating scheme to update the disparity estimation. There are two main steps in each round of updation. At first new reliable points are progressively selected based on three aspects of criterion including matching degree, confidence, and left–right consistency; then prediction-based growing matching is adopted to recalculate the disparity map from the reliable points. Finally, the more accurate depth map can be obtained by subpixel interpolation and transformation. The experimental results well demonstrate the effectiveness and low computational cost of our scheme.

OCIS codes: 150.6910, 330.1400.

1. Introduction

Among all three-dimensional (3D) depth reconstruction methods, the speckle projection system [1–5] has attracted a lot of attention and gained development for its good performance and low cost recently. It projects a speckle pattern to the objects in the scene, and then computes the dense depth information through triangulation geometry. Chen and Chen [1] built up a binocular system with two cameras to capture the stereo image pair of the projected speckle pattern, and directly applied stereo matching to compute the depth for near surfaces. Similar to Chen's system setup, Schaffer *et al.* [2] replaced the projector with a laser and a diffuser, and did the depth estimation based on a combination of the temporal correlation technique and the areal correlation technique (ACT). However, the system required high-speed cameras and a powerful processing platform. Dai and Su [3] captured and saved a series of speckle pattern images of planes with fixed depth beforehand; thus they can estimate scene depth by matching with the reference set only using a single camera. More recently, Freedman *et al.* [4] and Shpunt and Zalevsky [5] employed an infrared laser speckle projector and an infrared camera, not only to eliminate the impact of the appearance of objects under visible light, but also to expand the range of depth perception, which greatly improved the practicality.

Since the speckle projection system is actually a quasi-binocular system, the depth result can be calculated by stereo matching. The stereo-matching algorithm on visible view has been a popular research topic in computer vision for decades. Scharstein and Szeliski [6] presented a detailed survey on the algorithms. But the stereo-matching algorithm cannot be applied to speckle images straightforward. For speckle images, the local intensity is in high contrast, and also there is no *a priori* knowledge of color segmentation. A lot of stereo-matching algorithms will fail in this case. In [1–4] they generally used the local window-based correlation matching algorithm. However the conventional methods are not suitable for the speckle imaging system, which will produce a lot of mismatches.

1559-128X/13/030516-09$15.00/0

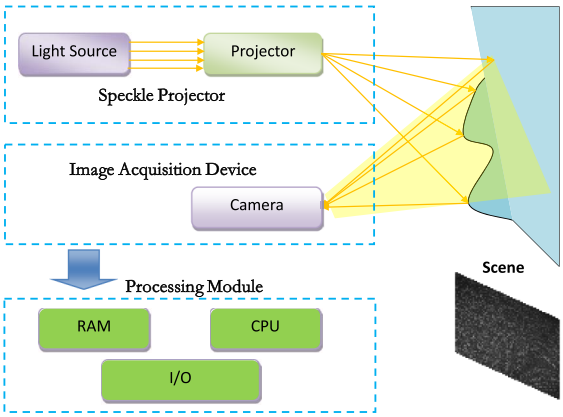

Fig. 1. (Color online) Structure of a typical speckle projection system.

In this paper we focus on fast indoor applications, which require only enough accuracy but relatively high speed. Considering the simplicity and relatively low computational cost of the ACT method, we propose a new ACT depth-estimation algorithm for the speckle projection system, based on self-adapting binarization (SAB) and progressive reliable points growing matching (PRPGM). First, our algorithm extracts the information of speckle by SAB on both the target image and the reference image. Then a local window-based correlation matching is applied to get the initial disparity estimation. By loosening the criterion parameters stepwise, we progressively select reliable points based on three measurements: matching degree, confidence, and left–right consistency (LRC). From the reliable points, we introduce a prediction-based growing matching method to update the disparity values. Finally, the more accurate depth map is obtained by subpixel interpolation and transformation. The experiments demonstrate the accuracy and effectiveness of our algorithm.

The rest of this paper is organized as follows: Section 2 briefly describes the motivation behind the design of our method and shows the framework. Section 3 describes our proposed algorithm in detail. Section 4 presents the experimental results and analysis. In the last section, we present a conclusion and a discussion of the future work.

2. Motivation and Framework

Our system is a combination of Scharstein's and Chen's; laser and diffuser are taken to project patterns onto the scene and a single camera is used to capture the speckle image. Figure 1 gives a typical speckle projection system including three modules: speckle projector, image acquisition device, and depth computation. In this paper, we assume that the system has been configured and calibrated so that the axis passing through the centers of the projector and the camera is parallel to the x-axis of the image sensor. With the ideal binocular triangulation geometry, the local speckle pattern shifts along the x-axis of the image as the depth value of the scene changes. Finally depth can be calculated through this shift value, say disparity.

The input data of the system consists of a real-time acquired target speckle image and a fixed reference speckle pattern. The reference image is a flat plane perpendicular to the optical axis, captured at a certain distance. Depth information is estimated by stereo matching between the target image and the reference image. Figure 2 shows one illustrative input image pair. In practical application, the unstable pulse of laser speckle, the image noise, and the radiometric variation within large range usually critically spoil the result. Besides, non-Lambertian surfaces, such as the window in Fig. 2, and out-of-range objects, significantly affect the accuracy of the depth map. Traditional stereo-matching methods cannot lead to an acceptable result.

To cope with above problems, we propose a novel algorithm, called PRPGM. Through classifying the matches into reliable and unreliable points, we recalculate the disparity values for those unreliable points by region growing manner. To alleviate the influence of the controls parameter, we begin the growing matching procedure with strict thresholds, then loosen them step-by-step and continue the growing process progressively. With this progressive growing scheme, unreliable matches in both bright foreground and dark background can be well updated.

Figure 3 depicts our scheme framework, including six main modules. The first step preprocesses the input image and computes a binary image that reflects

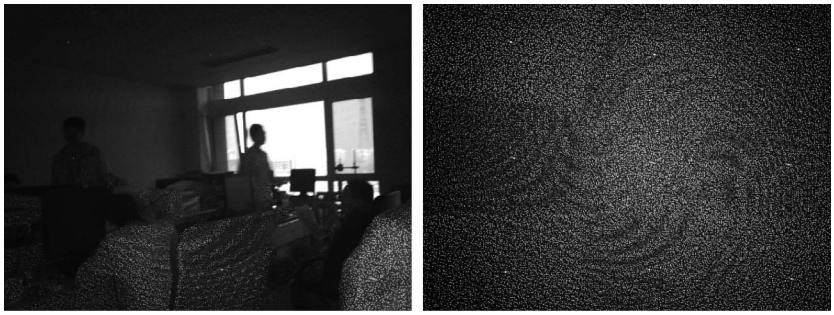

(a) (b)

Fig. 2. Illustration of a typical input image pair of laser speckle projection system. (a) Target speckle image and (b) reference speckle image.

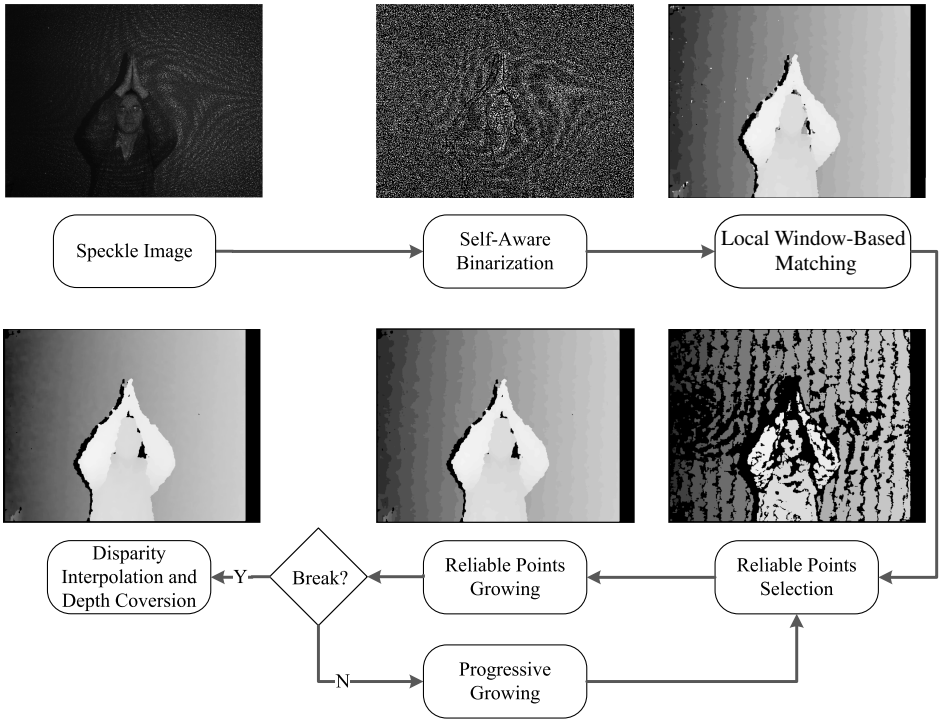

Fig. 3. Flow chart of proposed PRPGM with samples.

the essential speckle pattern. Then we calculate the disparity space image and initialize the disparity map by a winner-take-all (WTA) strategy. After the initialization, reliable points are selected according to three aspects, including matching degree, confidence, and LRC. This is followed by the prediction-based growing matching modules. It is noted that the threshold of the reliable points is progressively adjusted in each round of updation of growing matching. Finally, the high-accuracy depth map is obtained by subpixel interpolation and transformation.

3. Details of PRPGM Algorithm

In this section we present the details of the proposed PRPGM method. Symbols of important notion are listed in Table 1.

A. Self-Adapting Binarization

In a speckle image, the local gray intensities of objects change along different depth. Different from the sub-block binarization in [1], we propose a SAB preprocessing method, which can better adapt to complex environments.

Table 1. Symbols and Explanations in this Section

Symbol	Explanation
$T(x,y)$	Self-adapting threshold
$f(x,y,d)$	Matching cost function
T_{fH}	High matching threshold for reliable points
T_{fM}	Middle matching threshold for growing matching
T_{fL}	Low matching threshold for growing termination
T_{Conf}	Confidence threshold
T_{LRC}	Left–right check threshold
Q	First in, first out (FIFO) queue of seed points

For any gray-scale image pixel $I(x,y)$, the binarization value $I'(x,y)$ can be expressed as

$$I'(x,y) = \begin{cases} 0, & \text{if } I(x,y) \le T(x,y) \\ 1, & \text{if } I(x,y) > T(x,y) \end{cases}. \tag{1}$$

$T(x,y)$ is the self-adapting threshold, which equals the mean value $\mu(x,y)$ of the gray scale of all pixels within the surround window centered at $I(x,y)$ with the size of $(2l+1)\times(2l+1)$, formulated by

$$T(x,y) = \frac{1}{(2l+1)^2}\sum_{s=-l}^{l}\sum_{t=-l}^{l} I(x+s,y+t). \tag{2}$$

With the SAB, the speckle pattern can be extracted accurately, as is shown in Fig. 4. Moreover, in this step, we simultaneously detect shadow area using a similar self-adapting way. Apply another binarization procedure to the input image using a different adaptive threshold $T'(x,y)$ written by

$$T'(x,y) = \mu(x,y) + \Delta c, \tag{3}$$

where Δc is a fixed positive offset. The shadow points are identified by measuring the local density of bright pixels in the latter binarization result. Figure 4 shows an example of the shadow mask we calculate.

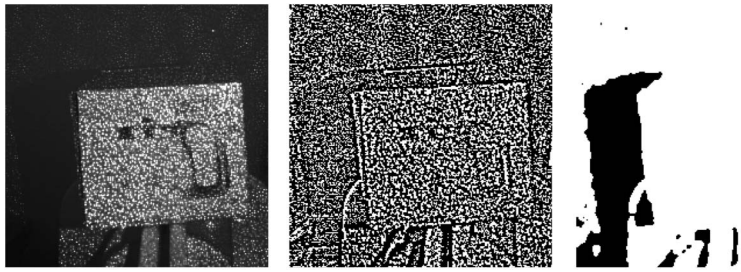

(a) (b) (c)

Fig. 4. Sample of SAB result. (a) Patch of input image, (b) results of SAB, and (c) calculated shadow mask.

B. Disparity Initialization

We use the traditional local window correlation-matching algorithm to initialize the disparity map.

Different from the normalized cross correlation (NCC) in [2], a simplified cost function is applied:

$$S(I1,I2) = \begin{cases} 1, & \text{if } I1 = I2 \\ 0, & \text{if } I1 \neq I2 \end{cases}. \tag{4}$$

All operations are integer arithmetic, which can avoid complicated and time-consuming floating-point number operations. In particular, for two binary valued pixels p and q, the similarity measurement can be computed by logical comparison. For any pixel p with the coordinate (x,y) in the target image L, its matching degree is defined as

$$f(x,y,d) = \frac{1}{N} \sum_{q \in \Omega(p)} S(L(x_q,y_q), R(x_q - d, y_q)), \tag{5}$$

where d indicates possible disparity, R is the reference image, $\Omega(p)$ is the aggregation window surrounding p, and N is the total number in the window.

We obtain the initial disparity for $p(x,y)$ by using the WTA [6] strategy as

$$D(x,y) = \underset{d\ \min \le d \le d\ \max}{\arg\max}\ f(x,y,d). \tag{6}$$

It is noted that we store the highest matching degree in $f_D(x,y)$.

C. Reliable Points Growing Matching

1. *Reliable Points Selection*

Because of noise and occlusion, the disparity with highest matching degree may not be accurate. The initial disparity map by local window matching usually has plenty of mismatches. To rectify these pixels, we put the local matching result into two categories: reliable points and unreliable ones. Under the depth continuity hypothesis, the disparity values of unreliable pixels can be predicted by growing matching with the reliable points.

The process of reliable points selection should meet the requirement that regions at different depth should have as many reliable points as possible. Therefore we evaluate the reliability of each disparity from three measurements: the matching degree, confidence, and LRC check.

The matching degree in Eq. (5) itself is a powerful measurement to distinguish reliable points. The higher the matching degree, the more reliable the result is.

In [7–9], the authors introduced the conception of confidence to describe the distinctiveness of the match. In a similar way, we define the confidence as the peak ratio of the maximum matching degree and the second maximum one:

$$\mathrm{Conf}(x,y) = \frac{f(x,y,D(x,y)) - \max_{d \neq D(x,y)} f(x,y,d)}{1 - \max_{d \neq D(x,y)} f(x,y,d)}. \tag{7}$$

With the help of the confidence criterion, we can exclude mismatches near depth discontinuous edges.

The LRC [6,10] is used in a lot of stereo-matching algorithms as a postprocessing step to refine the disparity map. Here we use it as the third standard. To be compatible with subpixel accuracy, we define the LRC value as the absolute difference between the results of twice matching, given by

$$\mathrm{LRC}(x,y) = |D_{L-R}(x,y) - D_{R-L}(x - D_{L-R}(x,y), y)|. \tag{8}$$

The left–right check can effectively detect occlusion, and eliminate the mismatches in the shadow area.

Considering the above three criteria, we select the points the meet all these conditions from the local matching result as the reliable points set:

$$R\mathrm{Set} = \left\{ (x,y) \middle| \begin{array}{l} f(x,y,D(x,y)) \ge T_{\mathrm{fH}} \\ \mathrm{Conf}(x,y) \ge T_{\mathrm{Conf}} \\ \mathrm{LRC}(x,y) < T_{\mathrm{LRC}} \end{array} \right\}, \tag{9}$$

where T_{fH}, T_{Conf}, and T_{LRC} are thresholds for the selection in matching degree, confidence, and LRC, respectively.

The speckle pattern may look different on different surfaces. Points on planes that face to the camera may have higher matching degree and confidence and lower LRC. They are selected as reliable points. In contrast, points in other areas, such as sharp

edges, are treated unreliable. Their depth can be estimated by the method described later.

2. Growing Matching

Depth continuous assumption is that adjacent pixels more than likely have the same depth. In most parts of the scene, depth values are continuous. Thus the unreliable points can be estimated by growing matching from neighboring reliable pixels. The steps are as follows:

1. Set a middle threshold T_{fM} and a low threshold T_{fL} of matching degree.
2. Create a FIFO queue Q; add the boundary points of the reliable points set in Q as seeds.
3. Pop a seed point p from Q, whose coordinates are (x_0, y_0) and disparity is d_0.
4. Consider each neighbor of p including $(x_0, y_0 - 1)$, $(x_0, y_0 + 1)$, $(x_0 - 1, y_0)$, and $(x_0 + 1, y_0)$. If it is unreliable, recalculate its disparity d and the matching degree f using WTA within the range of $d_0 - 1$, d_0, $d_0 + 1$.
5. If $f \geq T_{\mathrm{fM}}$, label it as a reliable point and add it in Q; if $T_{\mathrm{fL}} \leq f < T_{\mathrm{fM}}$, label it as an unknown point and update the matching record if f is higher than previous $f_D(x, y)$; if $f < T_{\mathrm{fL}}$, this growing is invalid.
6. Go to step 3 until Q is empty.

By this growing matching, the mismatches in regions within the perception range get refined, and the areas that exceed the depth-mapping range can be identified by the growing interruption scheme naturally, which is the main advantage of this method. Meanwhile the competition mechanism on the matching degree during the growing course ensures the correct matching for pixels near depth edges.

D. Progressive Growing Scheme

Although the reliable points growing scheme can effectively reassign correct disparity values to those unreliable points, the performance is sensitive to the parameters, especially the thresholds for reliable points selection. For example, if the thresholds are tightly set, the reliable points are too few to spread its context (depth) and reassign to the unreliable regions. But if we loosen the parameters to make more points reliable points, the mismatched points may be included in the reliable set and diffuse the disparity error. It is observed that the matching measure of pixels at near depth is usually higher than that at far pixels due to the variation of the speckle contrast. Therefore our growing scheme aims to reassign the disparity from near progressively.

At the first round, we set the thresholds T_{fH} and T_{Conf} with high values to strictly select the reliable matches. We also initialize T_{fM} to ensure the credibility of the prediction-based disparity reassignment. Then during each growing round, we stepwise loosen the requirement for reliable points selection as in the following equations:

$$T_{\mathrm{fH}}^{t} = T_{\mathrm{fH}}^{t-1} - \Delta T_{\mathrm{fH}}, \tag{10}$$

$$T_{\mathrm{Conf}}^{t} = T_{\mathrm{Conf}}^{t-1} - \Delta T_{\mathrm{Conf}}. \tag{11}$$

Correspondingly, in growing matching procedure, we also stepwise lower the threshold for reliability propagation:

$$T_{\mathrm{fM}}^{t} = T_{\mathrm{fM}}^{t-1} - \Delta T_{\mathrm{fM}}. \tag{12}$$

The reliable points are retained while the number of unreliable points is decreased during each round. To make the updation stable, the high matching threshold T_{fH} for the final round should not be lower than the initial T_{fM}. Thus we decide the number of growing rounds n by this constraint:

$$T_{\mathrm{fH}}^{0} - n\Delta T_{\mathrm{fH}} >= T_{\mathrm{fM}}^{0}. \tag{13}$$

As the growing matching is proceeding progressively, the matching record is adjusted automatically with growth competition. At the last round, we identify the bad pixels from the unreliable points set by measuring the matching record. Thus we can reject the regions unable to match in the output depth map.

E. Disparity Interpolation and Depth Transformation

Interpolation is adopted to improve the precision of the disparity map. In [11] the authors compared four designs of interpolation function. We choose the linear interpolation method to achieve subpixel precision.

Suppose the integer disparity for any pixel is d, and the corresponding matching degree is $f(d)$. If $d \neq d\ \max$ and $d \neq d\ \min$, let $\Delta L = |f(d) - f(d-1)|$ and $\Delta R = |f(d) - f(d+1)|$, and define

$$x = \begin{cases} \frac{\Delta L}{\Delta R}, & \text{if } \Delta L \leq \Delta R \\ \frac{\Delta R}{\Delta L}, & \text{if } \Delta L > \Delta R \end{cases}. \tag{14}$$

Then the subpixel disparity d_{final} is calculated by

$$d_{\mathrm{final}} = \begin{cases} d - 0.5 + \mathrm{interpF}(x), & \text{if } \Delta L \leq \Delta R \\ d + 0.5 - \mathrm{interpF}(x), & \text{if } \Delta L > \Delta R \end{cases}, \tag{15}$$

where $\mathrm{interpF}(x)$ is the linear interpolation function, described as

$$\mathrm{interpF}(x) = \frac{x}{2}. \tag{16}$$

According to the triangular geometry, the relation between disparity d and the actual depth Z in Euclidean metric can be formulated as in the transformation below:

$$Z = \frac{sZ_0}{s + dZ_0}, \tag{17}$$

where s is a constant determined by the focal length of the camera and the distance between the center of

the speckle projector and the center of the camera lens, and Z_0 is the depth of the reference plane.

4. Experiments

To evaluate the performance of our PRPGM algorithm, we utilize the output low-resolution speckle image from Kinect and implement the proposed algorithm using C language under a desktop computer with 2.80 GHz Core2 i7-2600 CPU and 4G RAM. Parameter values are fixed as follows: $l = 4$, $\alpha = 0.2$, $\Delta c = 2.0$, $T_{\mathrm{fH}}^0 = 0.9$, $\Delta T_{\mathrm{fH}} = 0.02$, $T_{\mathrm{Conf}}^0 = 0.25$, $\Delta T_{\mathrm{Conf}} = 0.015$, $T_{\mathrm{fM}}^0 = 0.75$, and $\Delta T_{\mathrm{fM}} = 0.015$, $T_{\mathrm{LRC}} = 1.0$. We visually and quantitatively evaluate our method on datasets captured under various scenes by comparison with the NCC-based areal local window matching.

In this paper, the well-known stereo-matching error rate [6] is adopted as the quantitative evaluation standard. This error rate is indicated by the percentage of the bad pixels whose disparity error is more than the tolerance,

$$B = \frac{1}{N}\sum_{(x,y)}(|d_C(x,y) - d_T(x,y)| > \delta_d). \tag{18}$$

In the experiments, the disparity error tolerance δ_d is set as 1.0. We convert the depth value back to the disparity value using the inverse transform of Eq. (17) to calculate the error rate.

A. Module Analysis

To verify the effectiveness of the SAB module, we compare the results of conventional local window matching with and without the SAB. Figure 5 gives an illustration. It shows the original image pair and the results using a different preprocessing step and matching degree. The black pixels in the error map represent the wrong matches, and the gray pixels indicate the errors in shadow area. The sum of absolute differences (SAD)-based window matching directly on the original image pair fails because of the radiometric variation of the local intensity. The census transform first proposed by Zahib and Woodfill [12] is proved to be a good matching degree especially invariant to monotonic intensity distortions. However, it also cannot achieve an accurate and smooth result for the speckle image with high contrast and noise. The result obtained from simple local matching with the proposed binarization method demonstrates that the SAB method is an effective and robust preprocessing module for the speckle measuring system.

The progressive growing performance and the convergence rate are the two crucial factors concerned in our PRPGM algorithm. Figure 6 shows the progressive updating results of the proposed method on a typical scene, which contains objects in different depth and an absorbent surface (the display screen) unable to calculate depth. Through the results compared with the ground truth, it can be seen that most error pixels in the initialization are correctly reassigned by the progressive growing matching process. The obvious difference between the last round and the initialization shows that our method can effectively identify bad regions and stop growing matching. The curve of the error rate can quickly converge no more than 10 rounds, and the execution time for each process is dropping due to the decreasing of the number of unreliable points. So we choose to stop the growing procedure after the seventh round to get a balance between performance and speed.

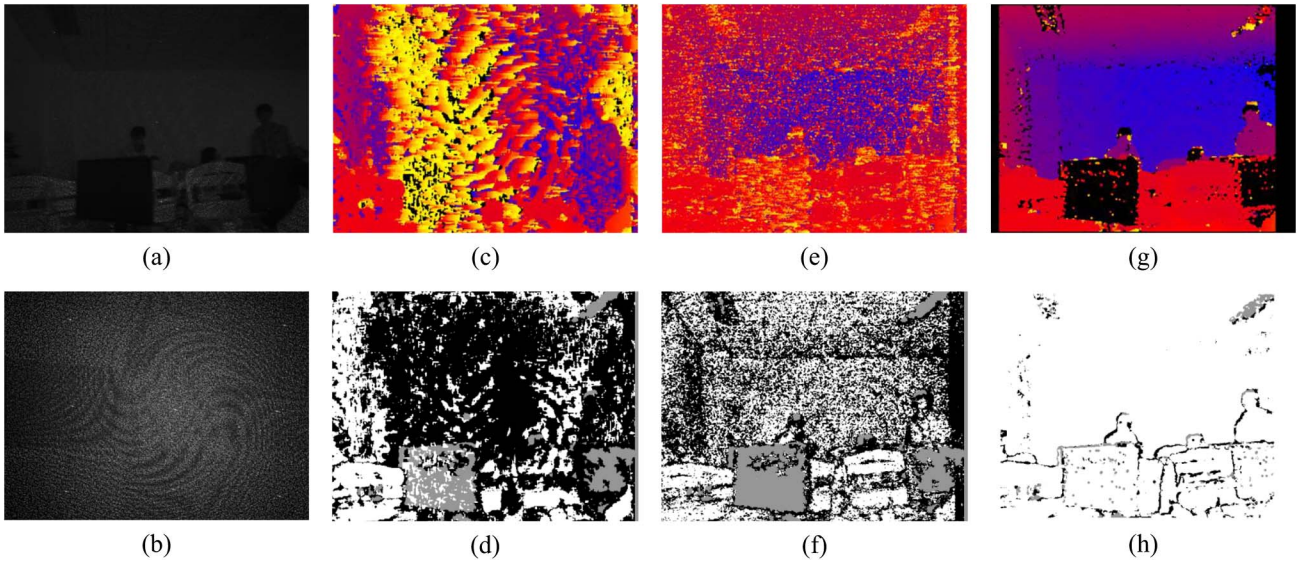

Fig. 5. (Color online) Illustration of the effect of SAB. (a) Original target image; (b) original reference image captured at a fixed distance; (c), (d) depth result from 13 × 13 local matching in original image using SAD and its error map; (e), (f) depth result using 13 × 13 census [12] and its error map; (g), (h) depth result from 13 × 13 window matching after SAB and its error map.

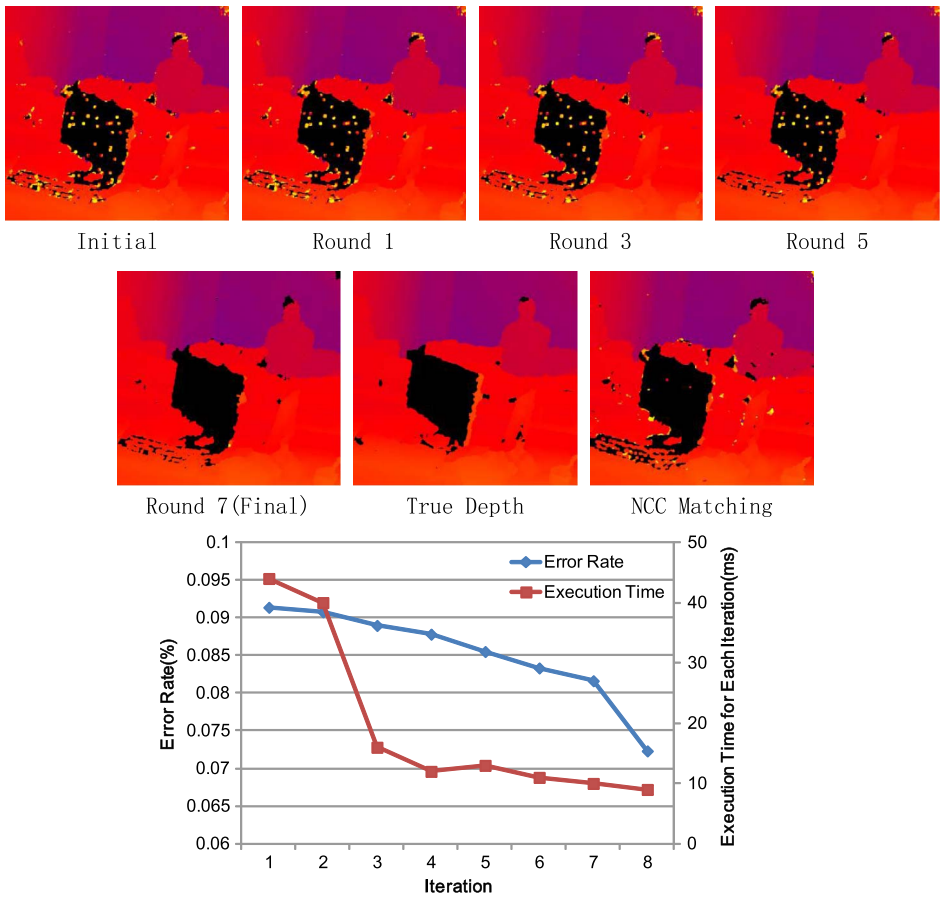

Fig. 6. (Color online) Results during the progressive growing rounds for a typical example. Upper: the intermediate depth results along with the progress, with the truth depth and NCC matching result as comparison. Lower: error rate and the execution time for each round.

B. Overall Performance

We designed the experiments to evaluate the overall performance of our proposed method, including plane test, surface depth estimation for near objects, and depth computation in the indoor environment.

First we capture speckle images for a series of planes perpendicular to the optical axis of the system at different distances, which means each of the plane has one unique depth value. The corresponding depth map is calculated by our proposed algorithm, where the root-mean-square error (RMSE) and the average relative error (ARE) are applied to measure the accuracy. The results are shown in Table 2 and Fig. 7. The AREs at different distances are all less than 2%, which verifies that our proposed algorithm achieves feasible accuracy and precision for different depth layers. According to the analysis in [13], the random error of depth measurement is proportional to the square distance from the sensor to the object. It can been seen in Fig. 7 that the RMSE

Table 2. Results of the Plane Test

Number	True Depth (mm)	Calculated Depth (mm)	RMSE (mm)	ARE (%)
1	557	557.4	2.04	0.29
2	918	916.2	3.34	0.35
3	1290	1290.3	4.99	0.32
4	1613	1613.9	11.5	0.56
5	2108	2115.2	17.3	0.70
6	2572	2578.1	24.0	0.76
7	2955	2972.7	32.1	1.10
8	3587	3641.2	36.1	1.56
9	4240	4311.2	68.7	1.91

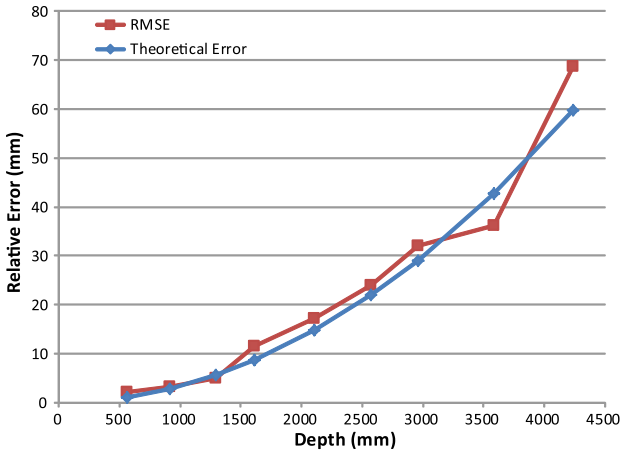

Fig. 7. (Color online) Comparison of proposed method's RMSE with theoretical error.

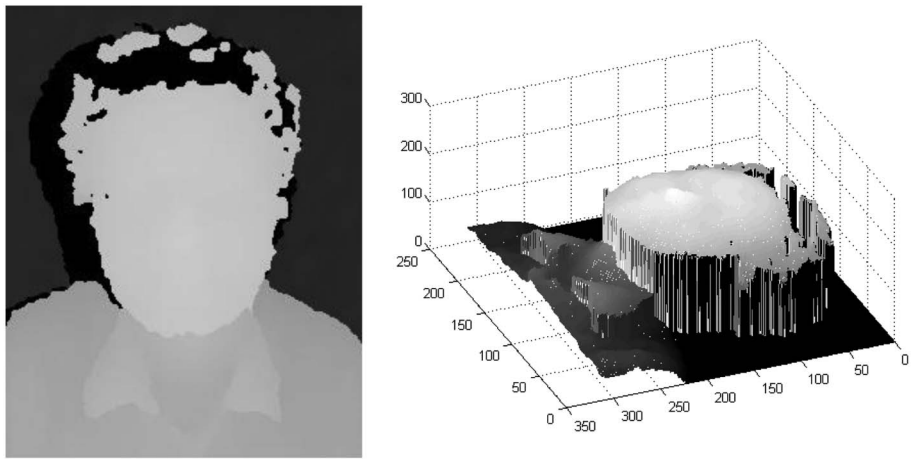

(a) (b)

Fig. 8. Depth estimation for human face surface. (a) Depth map produced by the proposed algorithm, and (b) synthesized view of the surface depth.

of proposed method coincides with the theoretical error computed from the method in [13].

We also examine our algorithm for surface depth estimation of near objects. In this experiment we choose a human face as the example. The face is about 0.8 m away from the sensor. We estimate the depth using the proposed algorithm and reconstruct the 3D model. Figure 8 shows the estimated depth map, where black pixels represent the hair and shadow area. The result is smooth and accurate, and there are almost no obvious error matching points. The unit of the depth direction Z-axis is millimeters (mm). Except for the side of the face that cannot been seen from the camera, the depth of the front of the face, the neck, the collar, and other particular parts of the face surface are all well estimated in spite of the limited precision of the system.

The most important application of our system is home entertainment. Therefore we experiment our method under different scenes in an indoor environment. We capture two speckle videos of different scenes with a relatively wide range and output the depth estimated by our algorithm. The calculated effective depth range is of 0.3–8.0 m. Key frames are illustrated in Fig. 9. The first scene is common, in which a user is making kinds of body movements in front of a wall under a slant view. The second scene is complex, captured using the system scanning around the whole environment, which contains plenty of complex background and areas out of the measuring range.

We compare our proposed method with NCC-based areal local window matching methods on the two datasets. In this experiment, the resolution of the input video and the output depth results is 640×480. The execution speed of the proposed algorithm under our unoptimized implementation is about 6 frames per second, which can be further accelerated utilizing

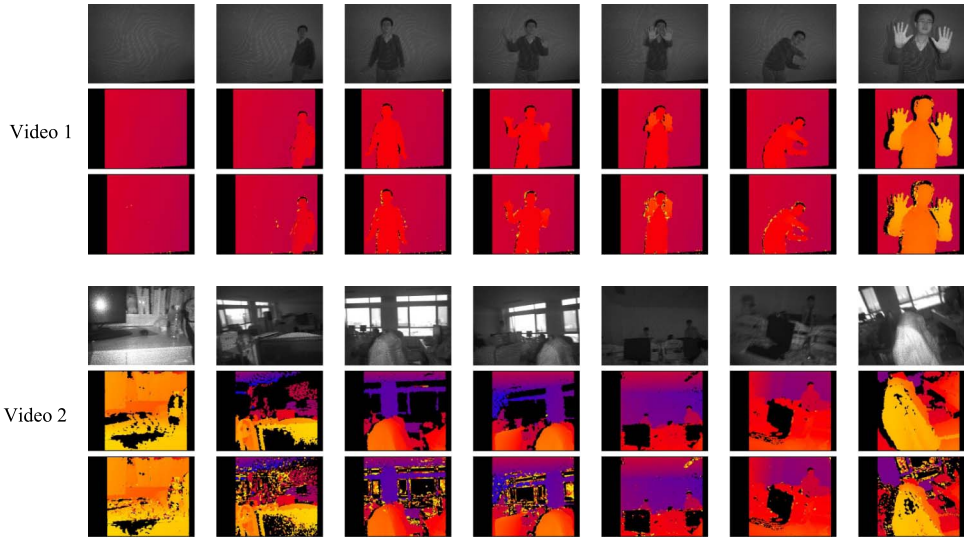

Fig. 9. (Color online) Some frames in our dataset videos. The upper row shows the captured IR speckle images, the middle row shows the result of NCC-based local window matching, and the bottom row shows the estimated depth with our method.

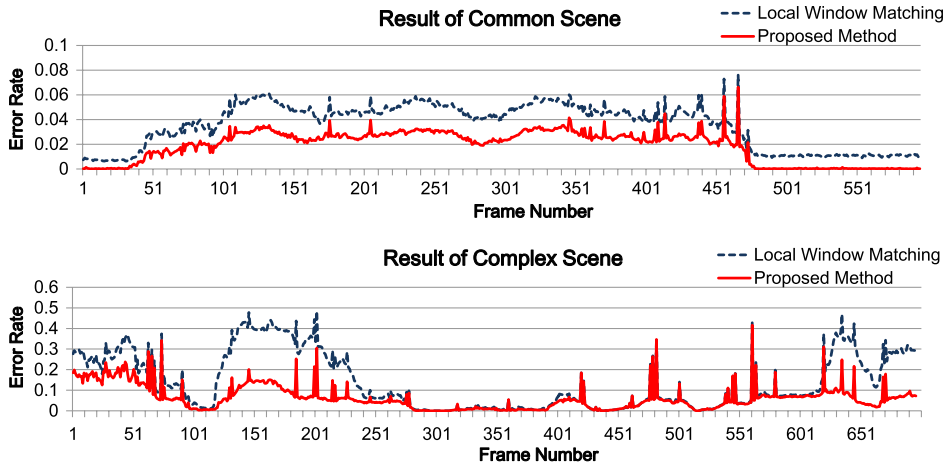

Fig. 10. (Color online) Comparison of the proposed algorithm with conventional method under different scenes.

a graphics processing unit. The results are diagramed in Fig. 10. As can be seen from the results, for the common scene, the error rate of our algorithm is less than 4% most of the time, which is significantly lower than the conventional algorithm. In the complex scene, the first 100 frames are captured too closely and the frames from 100 to 250 are too far, both of which are out of measuring range of the system. The traditional NCC-based matching algorithm cannot correctly identify the areas exceeding the range, leading to the depth results with many wrong matches. We can correct the mismatches and stop growing at the edges of those outranged areas. Our scheme can effectively identify them and output tags to avoid interference of the errors on those regions, thus dramatically improving the accuracy of the output depth results.

5. Conclusion

In this paper, a new depth-estimation algorithm for a speckle projection system is proposed, named PRPGM. In order to alleviate the effect of illumination inhomogeneity, a SAB step is introduced. We progressively select reliable points from the initial local matching result, and then use their information to re-estimate the depth of unreliable points. Finally we can get an depth map with feasible accuracy. Experiments demonstrate the effectiveness and robustness of our algorithm. Our algorithm meets the requirement of the laser speckle projection system and can be widely applied in depth ranging and 3D reconstruction.

As a future work, we plan to explore denoising methods to improve the initialization step and accelerate the matching process with the help of a parallel computing device.

This work was supported by National Natural Science Foundation of China (Nos. 61132007 and 61271390).

References

1. Y. Chen and B. Chen, "Measuring of a three-dimensional surface by use of a spatial distance computation," Appl. Opt. **42**, 1958–1972 (2003).
2. M. Schaffer, M. Grosse, and R. Kowarschik, "High-speed pattern projection for three-dimensional shape measurement using laser speckles," Appl. Opt. **49**, 3622–3629 (2010).
3. H. Dai and X. Su, "Shape measurement by digital speckle temporal sequence correlation with digital light projector," Opt. Eng. **40**, 793–800 (2001) (in Chinese).
4. B. Freedman, A. Shpunt, M. Machline, and Y. Arieli, "Depth mapping using projected patterns," U.S. patent 0,118,123 (13 May 2010).
5. A. Shpunt and Z. Zalevsky, "Three-dimensional sensing using speckle patterns," U.S. patent 0,096,783 (16 April 2009).
6. D. Scharstein and R. Szeliski, "A taxonomy and evaluation of dense two-frame stereo correspondence algorithms," Int. J. Comput. Vis. **47**, 7–42 (2002).
7. Q. Yang, L. Wang, R. Yang, H. Stewenius, and D. Nister, "Stereo matching with color-weighted correlation, hierarchical belief propagation, and occlusion handling," IEEE Trans. Pattern Anal. Mach. Intell. **31**, 492–504 (2009).
8. C. Shi, G. Wang, X. Pei, B. He, and X. Lin, "An interleaving updating framework of disparity and confidence map for stereo matching," IEICE Trans. Inf. Syst. **E95-D**, 1552–1555 (2012).
9. C. Shi, G. Wang, X. Pei, B. He, and X. Lin, "Stereo matching using local plane fitting in confidence-based support window," IEICE Trans. Inf. Syst. **E95-D**, 699–702 (2012).
10. K. Muhlmann, D. Maier, J. Hesser, and R. Manner, "Calculating dense disparity maps from color stereo images, an efficient implementation," Int. J. Comput. Vis. **47**, 79–88 (2002).
11. I. Haller and S. Nedevschi, "Design of interpolation functions for sub-pixel accuracy stereo-vision systems," IEEE Trans. Image Process. **21**, 889–898 (2011).
12. R. Zahib and J. Woodfill, "Non-parametric local transforms for computing visual correspondence," Proc. ECCV **801**, 151–158 (1994).
13. K. Khoshelham and S. Elberink, "Accuracy and resolution of kinect depth data for indoor mapping applications," Sensors **12**, 1437–1454 (2012).